Cell Reports
Medicine

Report

A High-Content Screen for Mucin-1-Reducing Compounds Identifies Fostamatinib as a Candidate for Rapid Repurposing for Acute Lung Injury

Graphical Abstract

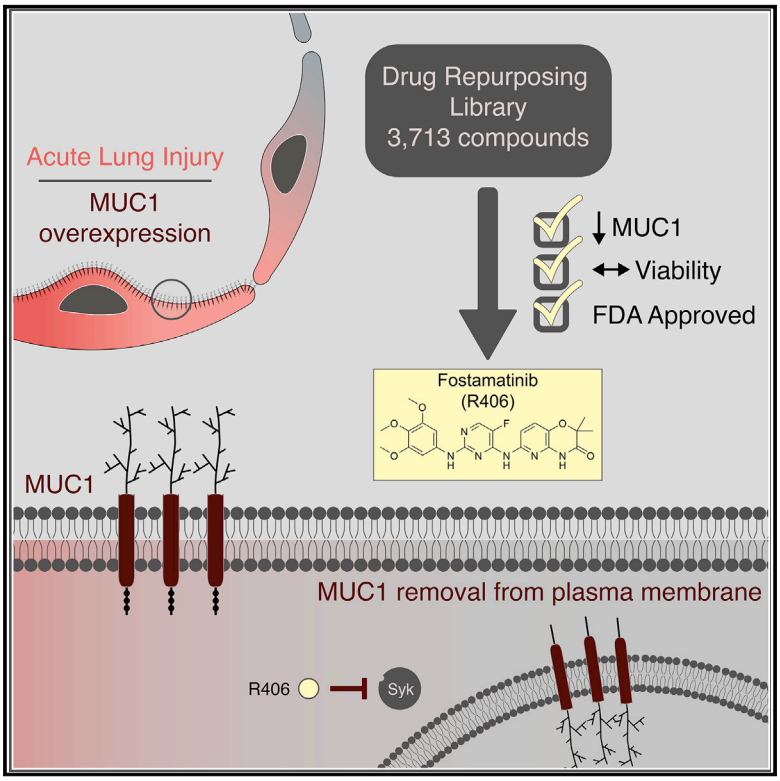

Highlights

- Elevated MUC1 levels predict the development of acute lung injury (ALI)
- A high-content screen of 3,713 compounds identifies repurposing candidates
- R406 removes MUC1 from the apical surface of epithelial cells
- Fostamatinib treatment reduces MUC1 in a mouse model of lung injury

Authors

Maria Kost-Alimova, Eriene-Heidi Sidhom, Abhigyan Satyam, ..., George C. Tsokos, Jillian L. Shaw, Anna Greka

Correspondence

agreka@bwh.harvard.edu

In Brief

In a high-content screen, Kost-Alimova et al. identify R406, the active metabolite of fostamatinib, as an FDA-approved candidate repurposing compound for the reduction of MUC1 protein levels in lung epithelium in the setting of acute lung injury.

Kost-Alimova et al., 2020, Cell Reports Medicine *1*, 100137
November 17, 2020
https://doi.org/10.1016/j.xcrm.2020.100137

CellPress

Cell Reports Medicine

CellPress
OPEN ACCESS

Report

A High-Content Screen for Mucin-1-Reducing Compounds Identifies Fostamatinib as a Candidate for Rapid Repurposing for Acute Lung Injury

Maria Kost-Alimova,[1,5] Eriene-Heidi Sidhom,[1,2,5] Abhigyan Satyam,[3] Brian T. Chamberlain,[1] Moran Dvela-Levitt,[1,2] Michelle Melanson,[1] Seth L. Alper,[1,3] Jean Santos,[1] Juan Gutierrez,[1] Ayshwarya Subramanian,[1] Patrick J. Byrne,[1] Elizabeth Grinkevich,[1] Estefanía Reyes-Bricio,[1] Choah Kim,[1,2] Abbe R. Clark,[1] Andrew J.B. Watts,[1,2] Rebecca Thompson,[1] Jamie Marshall,[1] Juan Lorenzo Pablo,[1] Juliana Coraor,[1,2] Julie Roignot,[1] Katherine A. Vernon,[1,2] Keith Keller,[1,2] Alissa Campbell,[1,2] Maheswarareddy Emani,[1] Matthew Racette,[1] Silvana Bazua-Valenti,[1,2] Valeria Padovano,[1] Astrid Weins,[2] Stephen P. McAdoo,[4] Frederick W.K. Tam,[4] Luciene Ronco,[1] Florence Wagner,[1] George C. Tsokos,[3] Jillian L. Shaw,[1] and Anna Greka[1,2,6,*]

[1]The Broad Institute of MIT and Harvard, Cambridge, MA, USA
[2]Brigham and Women's Hospital and Harvard Medical School, Boston, MA, USA
[3]Beth Israel Deaconess Medical Center and Harvard Medical School, Boston, MA, USA
[4]Department of Immunology and Inflammation, Imperial College, Hammersmith Hospital, London, UK
[5]These authors contributed equally
[6]Lead Contact
*Correspondence: agreka@bwh.harvard.edu
https://doi.org/10.1016/j.xcrm.2020.100137

SUMMARY

Drug repurposing has the advantage of identifying potential treatments on a shortened timescale. In response to the pandemic spread of SARS-CoV-2, we took advantage of a high-content screen of 3,713 compounds at different stages of clinical development to identify FDA-approved compounds that reduce mucin-1 (MUC1) protein abundance. Elevated MUC1 levels predict the development of acute lung injury (ALI) and acute respiratory distress syndrome (ARDS) and correlate with poor clinical outcomes. Our screen identifies fostamatinib (R788), an inhibitor of spleen tyrosine kinase (SYK) approved for the treatment of chronic immune thrombocytopenia, as a repurposing candidate for the treatment of ALI. *In vivo*, fostamatinib reduces MUC1 abundance in lung epithelial cells in a mouse model of ALI. *In vitro*, SYK inhibition by the active metabolite R406 promotes MUC1 removal from the cell surface. Our work suggests fostamatinib as a repurposing drug candidate for ALI.

INTRODUCTION

Drug repurposing is a strategy to identify novel uses for approved or investigational drugs outside the scope of their originally designated purposes. This approach offers several advantages over *de novo* drug development.[1,2] First and foremost, the risk of toxicity is much lower, as repurposed approved drugs have been proven safe for human use in the original indication. Second, and of critical importance for addressing the global public health crisis attributed to severe acute respiratory syndrome-coronavirus-2 (SARS-CoV-2), is that drug repurposing offers the only method for delivering treatments on the shortened timescale required to treat coronavirus disease 2019 (COVID-19) patients. The management of COVID-19 is at present largely supportive and with severely limited therapeutic options. Once infection with SARS-CoV-2 is established, a subset of patients experience severe complications such as acute respiratory distress syndrome (ARDS), an extreme form of ALI characterized by disruption to the alveolar epithelium.[3,4] ARDS is a life-threatening condition, with mortality rates as high as 40%.[5,6] COVID-19-associated ARDS is often fatal, especially in the presence of several preexisting conditions. The limited therapeutic interventions available for COVID-19[7,8] have contributed to an estimated 1 million deaths worldwide at the time of writing.[9] The identification of drugs with efficacy in treating ALI in severely affected COVID-19 patients remains an urgent need.

ARDS patients exhibit high serum levels of mucin-1/MUC1 (KL-6).[10] MUC1 is a transmembrane protein expressed on the apical membrane of most mucosal epithelial cells and plays a critical role in lining the airway lumen.[11] Mucins are glycoproteins that impart specific properties to mucus. In response to specific stimuli, goblet cells can rapidly secrete mucus by exocytosis to form a mucus layer that lines the airways. In healthy individuals, mucus along the lumen serves as a major protective barrier against inhaled pathogens, toxins, and other foreign particles. However, excessive mucus in the airways has been linked to increased frequency and duration of infections, decreased lung function, and increased mortality from respiratory diseases.[12] Abnormalities in mucus production contribute to severe pulmonary complications and death from respiratory failure in patients

with diseases such as cystic fibrosis, chronic obstructive pulmonary disease (COPD), and ALI due to viral pathogens such as SARS-CoV2. Elevated serum KL-6/MUC1 levels are an early prognostic marker of the therapeutic effect of high-dose corticosteroids in patients with rapidly progressing idiopathic pulmonary fibrosis.[13] Serum KL-6/MUC1 levels are also elevated in patients with interstitial pneumonitis.[14,15] Moreover, transgenic mice expressing human MUC1 and subjected to lipopolysaccharide (LPS)-induced ALI exhibit elevated KL-6 both in alveolar pneumocytes and in serum.[16]

Prompted by the connection between elevated MUC1 and ALI, we investigated the possibility of identifying MUC1-reducing drugs for rapid repurposing. We had originally screened the Broad Repurposing Library (composed of 3,713 compounds at different stages of pre-clinical and clinical development[17]) to identify compounds capable of reducing a mutant MUC1 neoprotein (MUC1-fs) causing autosomal dominant tubulo-interstitial kidney disease-*mucin1* (ADTKD-*MUC1* or *MUC1* kidney disease, MKD).[18] In this context wild-type MUC1 (MUC1-WT) served as a control, as we sought compounds that specifically reduced the mutant, but not the WT form of MUC1. As the number of COVID-19 cases increased globally, we turned our attention to identifying MUC1-reducing compounds and mined this dataset to identify approved drugs that reduce the expression of MUC1-WT. We searched for MUC1-reducing compounds based on the following criteria: (1) a drug that reduces MUC1-WT protein in a dose-dependent manner; (2) a drug with a favorable toxicity profile; (3) a drug that reduces MUC1-WT by non-transcriptional mechanisms,[18] unlike transcriptional suppressors such as vitamin D agonists that have proven ineffective in the clinic[19]; and (4) a drug that is US Food and Drug Administration (FDA) approved. Based on these criteria, our screen identified R406, the active metabolite of fostamatinib (R788, an oral prodrug rapidly converted to R406), as a repurposing candidate for the treatment of ALI.

RESULTS

R406, the Active Metabolite of FDA-Approved Fostamatinib, Depletes MUC1 from Epithelial Cells without Affecting Cell Viability

To investigate the expression pattern of MUC1 in human tissue, we took advantage of the openly available Human Protein Atlas (HPA) (http://www.proteinatlas.org).[20] Immunoperoxidase staining of human lung showed MUC1 expression in alveolar epithelium. This finding confirmed multiple reports of MUC1 expression in normal and diseased human lung (Figure 1A).[21,22] These data were corroborated by the expression of MUC1 mRNA in human lung reported by the HPA, Genotype-Tissue Expression (GTEx), and FANTOM5 databases (Figure 1B) and by the Human Lung Atlas project.[23]

We screened 3,713 compounds of the Repurposing Library for their ability to reduce MUC1 protein levels (Figure 2A). The screen used high-content immunofluorescence (IF) imaging of an immortalized kidney tubular epithelial cell line (P cells) that express endogenous MUC1 on the plasma membrane, to simultaneously assess MUC1 protein abundance and cell number as an index of cell toxicity.[18] The bromodomain inhibitor JQ1 served as a positive control, as preliminary experiments demonstrated complete transcriptional suppression of MUC1 by JQ1. Each compound in the Repurposing Library was tested in a 5-concentration, 10-fold dilution series with a top concentration of 35 μM in the initial screen. Positive hits from the 5-dose screen were defined by 2 criteria: lack of cellular toxicity (<20% reduction in cell number compared to the DMSO control); and reduction of MUC1 abundance by >30% (normalized to DMSO and JQ1 controls) at ≥2 consecutive non-toxic concentrations of the test compound. The compounds that met these criteria included 2 major groups, bromodomain inhibitors (blue) and vitamin D receptor agonists (orange, Figure 2B). Our screen also identified drugs that increased MUC1 levels (Figure 2B), including glucocorticoid receptor agonists. Most compounds that increased MUC1, such as epidermal growth factor receptor (EGFR) inhibitors (green), also reduced the cell number, indicating an association between cell toxicity and increased MUC1 levels (Figure 2B).

A total of 203 compounds were re-tested at 10 concentrations to generate more complete dose-response curves for each compound. In this screen, any compound that reduced MUC1 by >30% at ≥2 consecutive concentrations without evidence of toxicity (cell numbers within 20% of the DMSO control) was considered a positive hit. Thirteen hits from this screen were analyzed further in secondary profiling assays, including quantitative PCR (qPCR) and cell viability screens. MUC1 qPCR (Figure 2C) showed that for most compounds, reduction of MUC1 protein abundance (MUC1 IF) was highly correlated with parallel reductions in mRNA abundance (MUC1 qPCR). Of interest, 4 compounds reduced MUC1 protein without affecting MUC1 mRNA. These included the spleen tyrosine kinase (SYK) inhibitor R406 (red, Figure 2C), the RAF inhibitor LGX818 (violet, Figure 2C), the mannosidase inhibitor Kifunensine (green, Figure 2C), and the IKK inhibitor TPCA-1 (turquoise, Figure 2C). None of these 4 compounds exhibited detectable toxicity (cell death or apoptosis) at any of the identified active concentrations. More important, only the SYK inhibitor R406 is FDA approved (Figures 2A and 2D). No additional compounds with known activity against SYK met our screening criteria. R406 decreased MUC1 protein abundance in cells with a half-maximal effective concentration (EC_{50}) of ~200 nM (representative images of cells treated with R406 at a range of concentrations; Figure 2E). The lack of effect on MUC1 mRNA levels (as shown by qPCR) indicated that MUC1 protein reduction was not achieved via transcriptional repression. The parent molecule of R406, fostamatinib (R788), showed no activity in the initial 5-concentration screen, as we would expect for a cell-based assay, because the prodrug (R788) contains a highly polar phosphate that makes R788 cell impermeable.

To probe the specificity of our findings and whether the activity observed with R406 can be attributed to a class effect, 6 additional SYK inhibitors were sourced and tested in the high content imaging assay, as described in Table 1. In addition to R406, this series of compounds included 4 compounds studied in Phase II clinical trials (TAK-659, GS-9973, PRT062070, and BIIB057), 1 compound studied in Phase I clinical trials (R112), and a pre-clinical compound (BAY-61-3606). All of these compounds are reported to have *in vitro* SYK inhibition of half-maximal inhibitory

CellPress
OPEN ACCESS

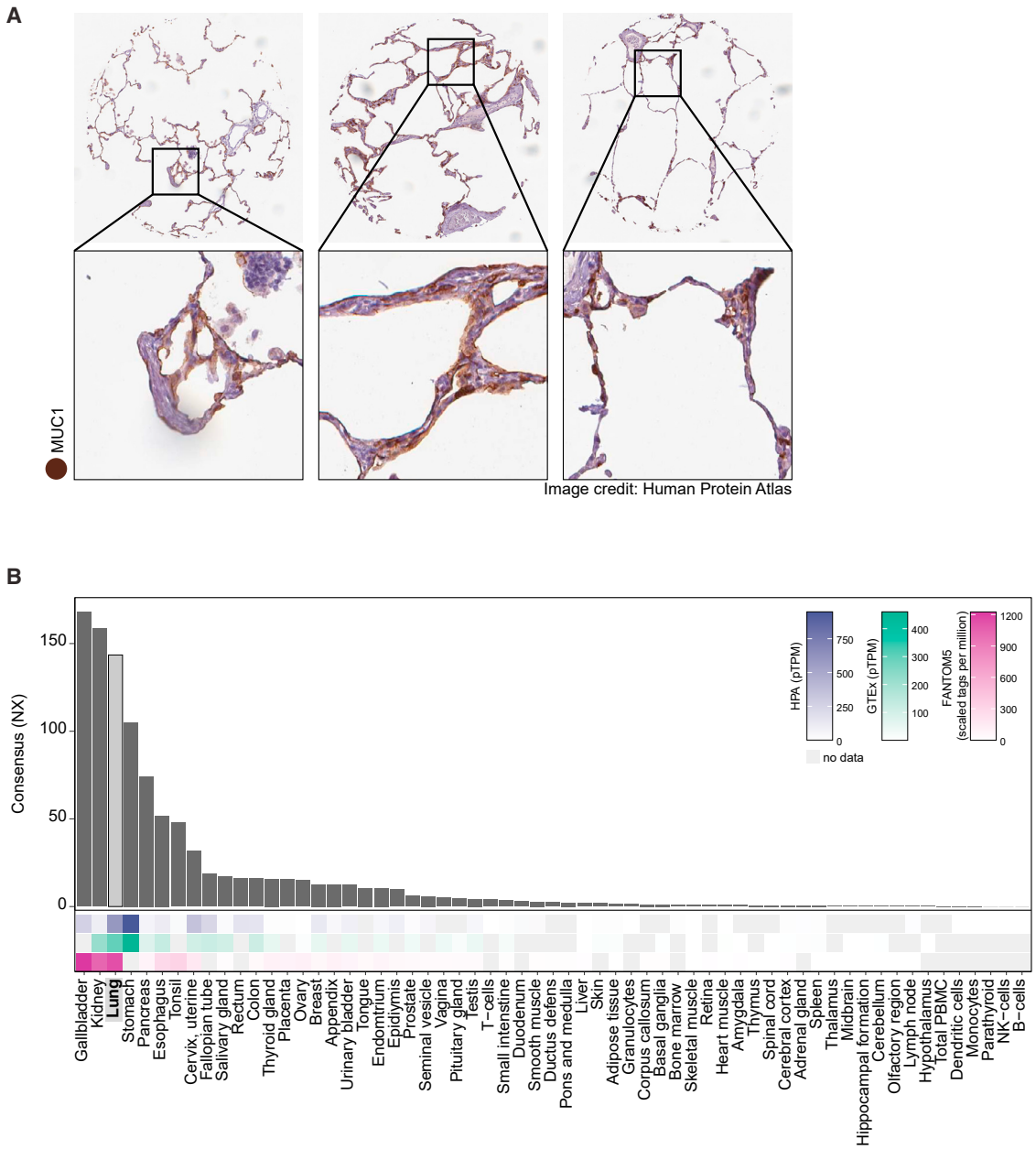

Figure 1. High Relative Expression of MUC1 in Human Lung

(A) Immunoperoxidase staining of 3 human lung samples demonstrates MUC1 protein abundance in lung tissue.

(B) mRNA expression data from 3 datasets (HPA, GTEx, and FANTOM5, heatmaps) combined into a CONSENSUS normalized transcript expression level (bar plot) show enhanced expression of MUC1 mRNA in human lung. NX, normalized expression; pTPM, protein-coding transcripts per million.

concentration (IC_{50}) < 100 nM. A range of activities was observed from weakly active (BIIB057) to ~200 nM (R406). No correlation between the SYK inhibition *in vitro* IC_{50} and the reduction of WT MUC1 EC_{50} was observed. Additional analyses to study the kinase specificity, or cell permeability, of these compounds could shed light on the wide range of WT Muc1 EC_{50}s, with potential implications for the effectiveness of specific syk inhibitors in clinical trials. Notably, R406 was the most potent compound in this panel and is the only active form of an approved drug.

R406 Preferentially Depletes MUC1 from the Plasma Membrane

Image analysis from the high-content screen revealed that while MUC1 was preferentially localized to the plasma membrane in DMSO-treated control cells, treatment with R406 (200 nM) reduced MUC1 from the plasma membrane and increased the fraction of protein found intracellularly in a perinuclear distribution pattern (Figure 3A). We quantified this relocalization using a STAR morphology "profile" module (STAR Methods) that

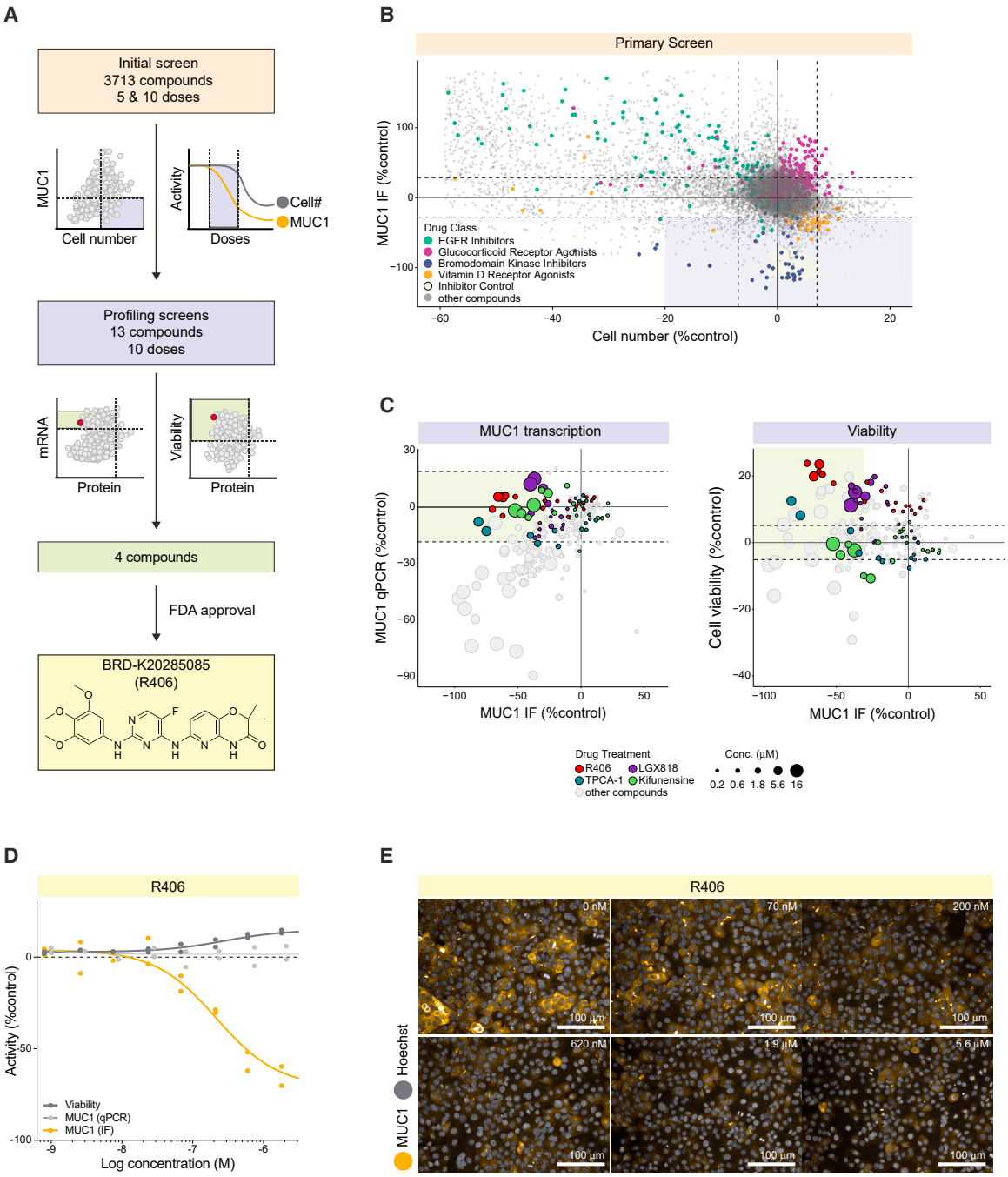

Figure 2. High-Content Screening Reveals Significant and Dose-Dependent Reduction in MUC1 by the FDA-Approved SYK Inhibitor R406

(A) Screening pipeline.

(B) Primary screen revealed 4 major groups of compounds that affected MUC1 levels. MUC1 immunofluorescence (IF) signal intensity per cell (normalized to positive control JQ1 minus DMSO-treated controls) plotted versus DMSO-normalized cell number. Horizontal and vertical dashed lines delineate mean DMSO values ± 3*SD for both MUC1 intensity and cell number. Lavender-shaded area demarcates candidate MUC1 suppressors.

(C) qPCR and cell viability profiling screens identified 4 compounds that reduced MUC1 protein abundance without changing MUC1 mRNA level, and in the absence of cytotoxicity for the previously identified active concentrations (the concentrations, which showed decrease in cell number in the initial screen, were removed from this analysis). Left: MUC1 signal intensity per cell plotted versus MUC1 mRNA level (qPCR assay). Both parameters are normalized to JQ1 minus DMSO-treated controls. Right: JQ1 minus DMSO-normalized MUC1 signal intensity per cell plotted versus DMSO-normalized cell viability (a number of viable cells after 6 days' exposure to the test compounds). Horizontal dashed lines delineate SD for DMSO-treated control wells for both cell viability and MUC1 qPCR. Green-shaded areas demarcate candidate hits.

(D) R406 concentration response curves for MUC1 protein abundance (orange), MUC1 mRNA abundance (light gray), and cell viability (dark gray).

(E) MUC1 IF in kidney epithelial cells treated for 48 h in the absence (DMSO) and presence of R406 at the indicated concentrations.

Table 1. R406 Emerges as the Most Potent Syk Inhibitor across the High Content Imaging Assay

Compound Name	Alternate Name(s)	BRD ID	Clinical Phase	WT Muc1 EC_{50} (μM)	*In Vitro* IC_{50} (nM)	Reference
R406	–	BRD-K20285085	active form of approved fostamatinib (R935788)	0.06	30	10.1124/jpet.106.109058
TAK-659	–	BRD-K71500795	2	3.6	3.2	10.1016/j.bmcl.2016.10.087
GS-9973	entospletinib	BRD-K76719364	2	1.9	7.7	https://pubs.acs.org/doi/10.1021/jm500228a
PRT062070	cerdulatinib	BRD-K25835157	2	0.59	32	10.1124/jpet.114.218164
BIIB057	P505-15, PRT062607	BRD-K53734668	2	>5.6	1	10.1124/jpet.111.188441
R112	R926112	BRD-K23902832	1	1.0	96	10.1016/j.jaci.2006.05.023
BAY-61-3606	–	BRD-K53281329	pre-clinical	>5.6	7.5	10.1124/jpet.103.052316

All of these compounds, including TAK-659, GS-9973, PRT062070, and BIIB057, one compound studied in Phase I clinical trials, R112, and a pre-clinical compound, BAY-61-3606, are reported to have *in vitro* syk inhibition of $IC_{50} < 100$ nM. No correlation between the syk inhibition *in vitro* IC_{50} and the reduction of WT Muc1 EC_{50} was observed. Notably, R406 was the most potent compound in this panel and is the only compound which is an approved drug or the active form of an approved drug.

allowed selective measurement of MUC1 signal distribution in cellular sub-compartments. Figure 3B shows an analysis sequence for the sub-compartment corresponding to the cell region closest to the plasma membrane. Within each cell, the nucleus border was identified based on Hoechst staining (blue, second panel, Figure 3B) and the plasma membrane (orange, second panel, Figure 3B) was identified based on the MUC1 signal. The calculated STAR morphology "membrane profile" image was generated as illustrated in Figure 3B, panel 3 (STAR Methods). The calculated STAR membrane profile values for MUC1 in each well were compared with total cell MUC1 intensity (Figure 3C). As shown by a local regression, while most compounds that decreased MUC1 did not selectively affect MUC1 membrane localization, R406 produced preferential depletion of MUC1 from the plasma membrane region at all active concentrations.

In Vivo, R406 Reduces Lung Epithelial MUC1 in Mice with ALI

SYK inhibition has previously been shown to suppress both local and remote lung injury.[24] R788 (fostamatinib disodium) is a methylene phosphate prodrug of R406 suitable for oral administration.[25] To investigate whether the administration of R788 may ameliorate ischemia/reperfusion (I/R)-induced remote lung injury by reducing MUC1 levels from the plasma membrane in the lung epithelium, C57BL/6J mice were fed a chow diet containing 3 g/kg of R788 for 10 days. Immunohistochemical images obtained from formalin-fixed paraffin sections of lung tissues stained with MUC1, phalloidin, and DAPI demonstrated that I/R-mediated ALI induced increased levels of MUC1 in lung epithelium, which is consistent with previous reports that excess MUC1 is injurious.[16] Importantly, MUC1 was significantly reduced by treatment with R788 (Figure 4A). Quantitative image analysis confirmed the *in vivo* efficacy of R788 in reducing MUC1 in injured lung epithelium (Figures 4B and 4C).

DISCUSSION

In a high-content screen, we identified R406, the active metabolite of fostamatinib, as an FDA-approved candidate repurposing compound for the reduction of MUC1 protein levels in lung epithelium in the setting of ALI. R406 is a potent inhibitor of SYK, a cytosolic protein tyrosine kinase required for the expression of several proinflammatory cytokines.[26] SYK is expressed in most leukocyte populations, with roles in mediating signaling via classical immunoreceptors such as B cell receptors and Fc receptors.[27] SYK plays diverse roles in cellular adhesion, innate immune recognition, and platelet activation, and its central role in immune cell responses has made it a compelling target for the development of therapeutic agents. Over 70 patent filings describe small-molecule inhibitors of SYK developed for the treatment of diseases ranging from arthritis to asthma.[28]

Fostamatinib was approved in April 2018 by the FDA for the treatment of chronic immune thrombocytopenia (ITP), an autoimmune disease that results in low levels of circulating platelets.[29–32] Moreover, fostamatinib is an effective treatment in experimental animal models of severe inflammatory diseases, including immune glomerulonephritis[33,34] and vasculitis.[35] Phase II clinical trial results are expected assessing the effect of SYK inhibition in proliferative immunoglobulin A (IgA) nephropathy, an inflammatory kidney disease (NCT02112838). Fostamatinib has also been extensively studied and found to be safe in >3,000 patients with rheumatoid arthritis.[36] In a Phase III clinical trial,[37] fostamatinib was well tolerated at an oral dose of 100 mg twice daily. Mild or moderate adverse effects included diarrhea, hypertension, nausea, and an increase in alanine aminotransferase (ALT). These effects resolved spontaneously or with medical management, including antihypertensive or antimotility agents. This well-characterized clinical safety profile[38] makes fostamatinib a good candidate for rapid repurposing.

Our finding that R406 preferentially depletes MUC1 abundance in or near the plasma membrane is consistent with a

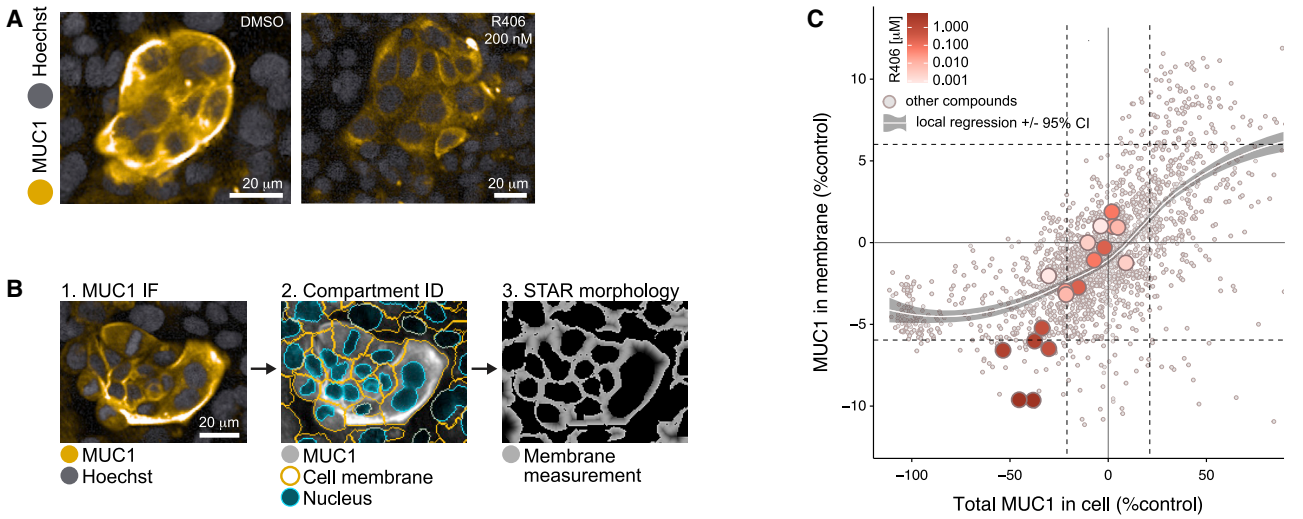

Figure 3. R406 Preferentially Depletes MUC1 from the Plasma Membrane

(A) R406 (at EC_{50} concentration) substantially reduced MUC1 abundance in or near the plasma membrane, with a portion of MUC1 retained in cytosolic and perinuclear cell compartments.

(B) Image analysis for cell compartmentation using STAR morphology "membrane profile" calculation (see STAR Methods). Image 1: cells with MUC1 preferentially localized at plasma membrane; image 2: Harmony software identification of nucleus (blue) and plasma membrane (gold) in each cell; image 3: STAR morphology membrane profile for the MUC1 predominant localization within the membrane compartment.

(C) STAR morphology membrane profile analysis of 203 compounds screened at 10 doses. R406 at most active concentrations reduced plasma membrane MUC1 abundance to a greater degree than most other compounds, as shown by deviation from the local regression. MUC1 IF signal intensity per cell (normalized to JQ1 minus DMSO-treated controls) plotted versus DMSO-normalized MUC1 predominance in plasma membrane region as calculated using the STAR morphology membrane profile module. Horizontal and vertical dashed lines delineate mean DMSO values ± 2*SD for both plotted parameters. Local regression was calculated by locally estimated scatterplot smoothing (loess) method ± 95% confidence interval (gray shaded).

previously described mechanism by which SYK inhibition results in the dephosphorylation of integral membrane proteins followed by their endocytic removal from the plasma membrane. For example, SYK signaling modulates cystic fibrosis transmembrane conductance regulator (CFTR) abundance in human airway epithelial cell plasma membrane.[39] Interestingly, in mucin-producing human NCI-H292 cells and in primary human nasal epithelial cells, SYK also regulates MUC5AC, a gel-like mucin that promotes lung epithelial injury.[40] In further support of the notion that MUC1 reduction is beneficial to injured lung epithelium, *Muc1* knockout in rat airway epithelial cells was protective against lung injury with cigarette smoke, and the knockdown of MUC1 in a human lung epithelial cell line (NCI-H292) was protective from cigarette smoke extract.[41] It remains to be determined how MUC1 reduction could confer benefit in a wide array of diseases, including cancer, in which MUC1 upregulation is frequently observed in circulating tumor cells from patients with advanced adenocarcinoma.[42]

Of more direct relevance to lung injury attributed to infection by SARS-CoV-2, a recent study identified elevated MUC1 and MUC5AC mucin levels obtained by bronchoscopy in the airway mucus of critically ill COVID-19 patients.[43] Furthermore, cytoplasmic MUC1 correlated with MUC1 on the plasma membrane of epithelial cells and with circulating MUC1 levels in the blood (due to detachment and disruption of the endothelial cells lining the alveolar capillaries).[43] These observations support a rationale whereby circulating MUC1 levels and increased intracellular and membrane MUC1 levels correlate with the severity of alveolar damage and overall lung disease, including COVID-19 lung disease.

Severe COVID-19 symptoms include viral-induced pneumonitis accompanied by prolonged, systemic cytokine release[44,45] in which levels of interleukin-6 (IL-6) levels and other cytokines and acute phase reactants correlate with respiratory failure. Macrophage-derived IL-6 upregulates MUC1 in the human colon cancer HT-29 cell line,[46] suggesting that a similar IL-6-mediated upregulation of MUC1 may occur in SARS-CoV-2-infected lungs. A recent comparison of 15 hospitalized COVID-19 patients, 9 of whom were critically ill, to 28 critically ill patients with ARDS or sepsis found no statistically significant difference in circulating levels of IL-1b, IL-1RA, IL-6, IL-8, and tumor necrosis factor α (TNF-α) among these conditions.[47] These results indicate that COVID-19-related ARDS is associated with inflammatory cytokine levels similar to those of ARDS due to other critical illnesses.[47] Another recent study analyzing serum concentrations of KL-6/MUC1 levels in hospitalized COVID-19 patients suggested KL-6/MUC1 as a good prognostic biomarker of disease severity in COVID-19 patients.[48] Given the roles of excess KL6/MUC1 in ALI and ARDS, we propose that fostamatinib may confer benefit in patients with COVID-19 lung injury.

Mechanistically, multiple studies of SARS and other acute viral respiratory infections are mediated by SYK-dependent events involving the activation of C-type lectin receptors (CLR) and immunoglobulin Fcγ receptors.[49] These SYK-mediated

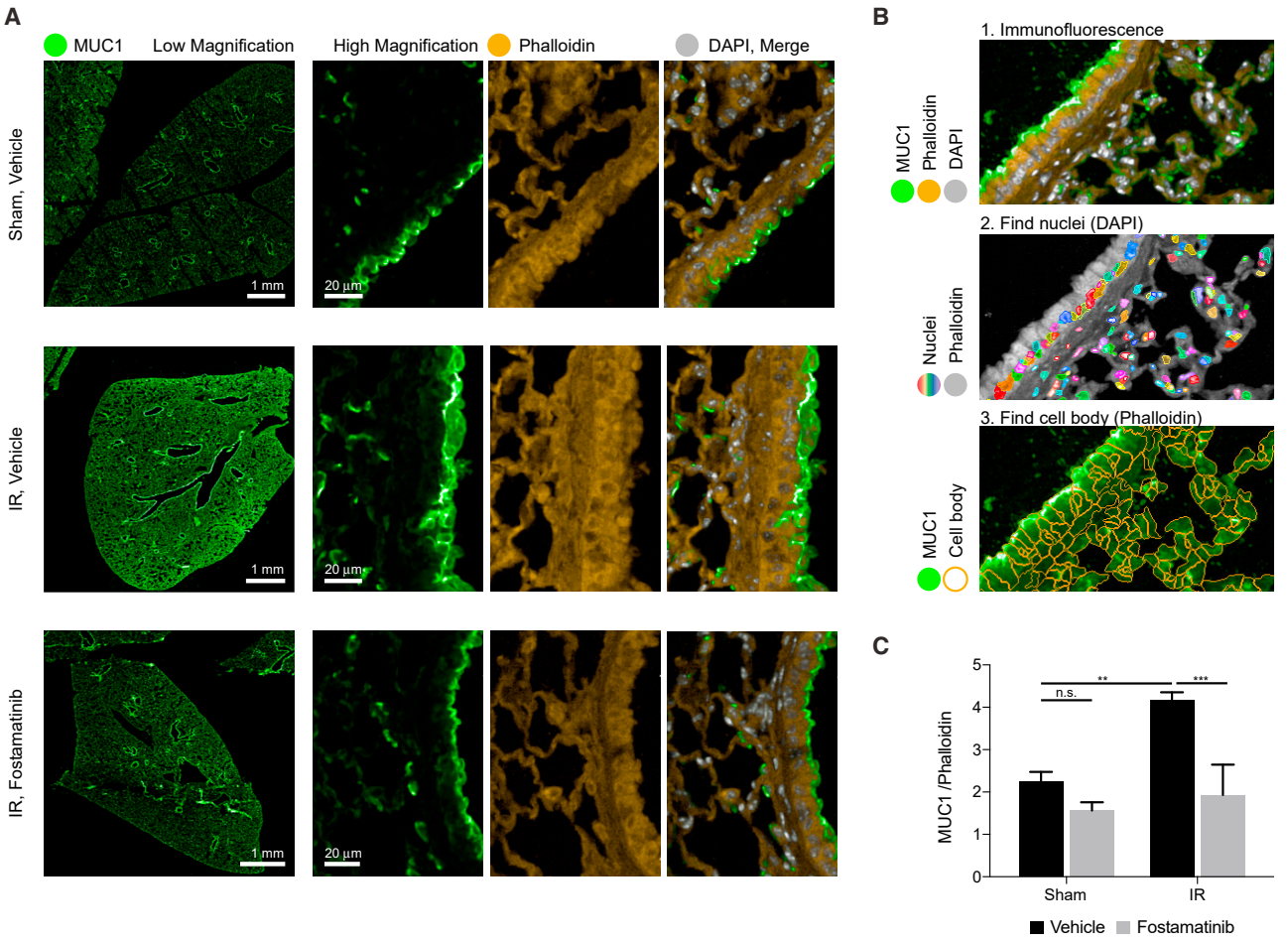

Figure 4. *In Vivo*, R788 Reduces Excess MUC1 from Lung Epithelia of Mice with ALI

(A) IF images from lung tissue sections stained with MUC1 (green), phalloidin (yellow), and DAPI (gray) demonstrate that ischemia/reperfusion (I/R)-induced remote ALI resulted in increased MUC1 in lung epithelium. Treatment with fostamatinib over the course of 10 days suppressed MUC1 levels in mouse lung epithelium.

(B) Single-cell tissue analysis, based on IF of MUC1 and phalloidin (panel 1). In each image (panel 1), nuclei were identified based on DAPI staining (rainbow colors represent different cell nuclei in panel 2). The cell bodies were identified based on phalloidin staining surrounding each nucleus (orange cell borders, panel 3). Lastly, MUC1 IF intensity (green in panel 3) and phalloidin intensities were calculated within each cell body.

(C) Bar graph ratio of MUC1:phalloidin intensities in all cells of tissue sections from sham-treated mice and mice subjected to I/R-induced ALI, treated either with or without fostamatinib. Average MUC1 intensity values per cell were normalized to the average phalloidin levels. Means ± SDs (n = 3 mice/condition/dose). ns, *p < 0.05, **p < 0.01, and ***p < 0.001.

processes result in inflammation, excessive cytokine and chemokine release, neutrophil activation, and endothelial cell stimulation that can lead to vascular endothelium leakage and edema in the lungs. These events contribute to ARDS, micro-thrombosis, and the associated systemic complications.[49] Additional data have recently emerged demonstrating that the observed hyper-inflammatory response induced by anti-Spike IgG from patients with severe COVID-19 could be specifically counteracted by the SYK inhibitor R406,[50] the same compound identified in our study. Anti-spike IgG from severely ill COVID-19 patients promoted inflammatory cytokines, endothelial barrier disruption, and microvascular thrombosis.[50] Furthermore, human macrophage activation in response to anti-SARS-CoV-2 IgG immune complexes recognized by Fcγ receptors (Fcγr) was shown to critically depend on SYK kinase for downstream signaling.[51,52] These studies suggest that the SYK inhibitor fostamatinib may provide a beneficial effect in acute COVID-19 lung injury by simultaneously targeting multiple pathways in both epithelial and immune cells.

In conclusion, our *in vitro* and *in vivo* data support the potential efficacy of fostamatinib for the treatment of ALI. In conjunction with additional emerging evidence suggesting that the observed hyper-inflammatory response induced by SARS-CoV-2 in patient lungs can be counteracted by the pro-drug of fostamatinib, our work provides a rationale for pursuing clinical trials to test whether repurposing this FDA-approved drug may have salutary effects for patients suffering from acute COVID-19 lung injury.

Limitations of Study

Our study has several limitations. First, we did not design this study with the primary intent to identify reducers of MUC1, but rather, with the purpose of finding reducers of a mutant version of this protein that is relevant to kidney disease. Nevertheless, our post hoc analysis of the dataset revealed fostamatinib as a candidate MUC1 reducer that protects from ALI in rodents. Second, we have not developed a deep mechanistic understanding of how the inhibition of SYK regulates MUC1 in lung epithelium. Our work here suggests that SYK-dependent internalization and sequestration of MUC1 from the plasma membrane may be one possible mechanism, but changes in MUC1 biosynthesis or degradation cannot be excluded, and will be the subject of future detailed studies. Finally, we have not established that the administration of fostamatinib is directly beneficial to ALI caused by SARS-CoV-2, as these studies would likely need to be performed in non-human primates, and this may not be necessary, given a well-established safety profile that affords us the opportunity to test the efficacy of this drug directly in patients.

STAR★METHODS

Detailed methods are provided in the online version of this paper and include the following:

- KEY RESOURCES TABLE
- RESOURCE AVAILABILITY
  - Lead Contact
  - Materials Availability
  - Data and Code Availability
- EXPERIMENTAL MODEL AND SUBJECT DETAILS
  - Cell Lines
  - Mice
- METHOD DETAILS
  - Broad Repurposing Library
  - Human Protein Atlas
  - Fluorescence image acquisition and analysis
  - High-Content Screening
  - Administration of SYK inhibitor R788
  - Mesenteric Ischemia-Reperfusion (I/R)
  - Immunohistochemistry
- QUANTIFICATION AND STATISTICAL ANALYSIS

ACKNOWLEDGMENTS

We gratefully acknowledge stimulating discussions with Broad Institute colleagues Deborah Hung, Ramnik Xavier, Jay Rajagopal, and Aviv Regev. We thank Terry Woo (BWH Pathology) and Stephen Straub (Perkin-Elmer) for excellent technical support and expertise. SYK inhibitor R788 was provided as a gift to G.C.T. by Rigel Pharmaceuticals. This work was supported by PHS NIH R01AI148161 (to G.C.T.) and by the Slim Initiative for Genomic Medicine in the Americas (SIGMA), a collaboration of the Broad Institute with the Carlos Slim Foundation. F.W.K.T. is supported by the Ken and Mary Minton Chair of Renal Medicine.

AUTHOR CONTRIBUTIONS

M.K.-A., A. Satyam, M.D.-L., M.M., J.S., and J.G. performed the experiments; M.K.-A., E.-H.S., A. Satyam, M.D.-L., B.T.C., and A. Subramanian performed the data analysis and provided data visualization; S.P.M., F.W.K.T., and G.C.T. provided tissue from and expertise in rodent models of lung disease; M.K.-A., E.-H.S., M.D.-L., B.T.C., J.S., and A.G. wrote the manuscript; all of the authors participated in discussions on the scientific rationale for this study and read and approved the manuscript; A.G. supervised the project.

DECLARATION OF INTERESTS

F.W.K.T. has received research project grants from and has consultancy agreements with Rigel Pharmaceuticals, and is the chief investigator of an international clinical trial of a SYK inhibitor in IgA nephropathy (ClinicalTrials.gov NCT02112838), funded by Rigel Pharmaceuticals.

Received: June 29, 2020
Revised: September 23, 2020
Accepted: October 13, 2020
Published: October 28, 2020

REFERENCES

1. Pushpakom, S., Iorio, F., Eyers, P.A., Escott, K.J., Hopper, S., Wells, A., Doig, A., Guilliams, T., Latimer, J., McNamee, C., et al. (2019). Drug repurposing: progress, challenges and recommendations. Nat. Rev. Drug Discov. *18*, 41–58.
2. Ashburn, T.T., and Thor, K.B. (2004). Drug repositioning: identifying and developing new uses for existing drugs. Nat. Rev. Drug Discov. *3*, 673–683.
3. Ruan, Q., Yang, K., Wang, W., Jiang, L., and Song, J. (2020). Clinical predictors of mortality due to COVID-19 based on an analysis of data of 150 patients from Wuhan, China. Intensive Care Med. *46*, 846–848.
4. Zhou, F., Yu, T., Du, R., Fan, G., Liu, Y., Liu, Z., Xiang, J., Wang, Y., Song, B., Gu, X., et al. (2020). Clinical course and risk factors for mortality of adult inpatients with COVID-19 in Wuhan, China: a retrospective cohort study. Lancet *395*, 1054–1062.
5. Determann, R.M., Royakkers, A.A., Haitsma, J.J., Zhang, H., Slutsky, A.S., Ranieri, V.M., and Schultz, M.J. (2010). Plasma levels of surfactant protein D and KL-6 for evaluation of lung injury in critically ill mechanically ventilated patients. BMC Pulm. Med. *10*, 6.
6. Rubenfeld, G.D., Caldwell, E., Peabody, E., Weaver, J., Martin, D.P., Neff, M., Stern, E.J., and Hudson, L.D. (2005). Incidence and outcomes of acute lung injury. N. Engl. J. Med. *353*, 1685–1693.
7. Cao, B., Wang, Y., Wen, D., Liu, W., Wang, J., Fan, G., Ruan, L., Song, B., Cai, Y., Wei, M., et al. (2020). A Trial of Lopinavir-Ritonavir in Adults Hospitalized with Severe Covid-19. N. Engl. J. Med. *382*, 1787–1799.
8. Grein, J., Ohmagari, N., Shin, D., Diaz, G., Asperges, E., Castagna, A., Feldt, T., Green, G., Green, M.L., Lescure, F.X., et al. (2020). Compassionate Use of Remdesivir for Patients with Severe Covid-19. N. Engl. J. Med. *382*, 2327–2336.
9. Dong, E., Du, H., and Gardner, L. (2020). An interactive web-based dashboard to track COVID-19 in real time. Lancet Infect. Dis. *20*, 533–534.
10. Nakashima, T., Yokoyama, A., Ohnishi, H., Hamada, H., Ishikawa, N., Haruta, Y., Hattori, N., Tanigawa, K., and Kohno, N. (2008). Circulating KL-6/MUC1 as an independent predictor for disseminated intravascular coagulation in acute respiratory distress syndrome. J. Intern. Med. *263*, 432–439.
11. Kato, K., Lillehoj, E.P., Lu, W., and Kim, K.C. (2017). MUC1: The First Respiratory Mucin with an Anti-Inflammatory Function. J. Clin. Med. *6*, 110.
12. Vestbo, J. (2002). Epidemiological studies in mucus hypersecretion. Novartis Found. Symp. *248*, 3–12, discussion 12–19; 277–282.
13. Yokoyama, A., Kohno, N., Hamada, H., Sakatani, M., Ueda, E., Kondo, K., Hirasawa, Y., and Hiwada, K. (1998). Circulating KL-6 predicts the outcome of rapidly progressive idiopathic pulmonary fibrosis. Am. J. Respir. Crit. Care Med. *158*, 1680–1684.

14. Ishikawa, N., Hattori, N., Yokoyama, A., and Kohno, N. (2012). Utility of KL-6/MUC1 in the clinical management of interstitial lung diseases. Respir. Investig. *50*, 3–13.

15. Kohno, N. (1999). Serum marker KL-6/MUC1 for the diagnosis and management of interstitial pneumonitis. J. Med. Invest. *46*, 151–158.

16. Sakai, M., Kubota, T., Ohnishi, H., and Yokoyama, A. (2013). A novel lung injury animal model using KL-6-measurable human MUC1-expressing mice. Biochem. Biophys. Res. Commun. *432*, 460–465.

17. Corsello, S.M., Bittker, J.A., Liu, Z., Gould, J., McCarren, P., Hirschman, J.E., Johnston, S.E., Vrcic, A., Wong, B., Khan, M., et al. (2017). The Drug Repurposing Hub: a next-generation drug library and information resource. Nat. Med. *23*, 405–408.

18. Dvela-Levitt, M., Kost-Alimova, M., Emani, M., et al. (2019). Small Molecule Targets TMED9 and Promotes Lysosomal Degradation to Reverse Proteinopathy. Cell *178*, 521–535.e3.

19. Castro, M., King, T.S., Kunselman, S.J., Cabana, M.D., Denlinger, L., Holguin, F., Kazani, S.D., Moore, W.C., Moy, J., Sorkness, C.A., et al.; National Heart, Lung, and Blood Institute's AsthmaNet (2014). Effect of vitamin D3 on asthma treatment failures in adults with symptomatic asthma and lower vitamin D levels: the VIDA randomized clinical trial. JAMA *311*, 2083–2091.

20. Uhlén, M., Fagerberg, L., Hallström, B.M., Lindskog, C., Oksvold, P., Mardinoglu, A., Sivertsson, Å., Kampf, C., Sjöstedt, E., Asplund, A., et al. (2015). Proteomics. Tissue-based map of the human proteome. Science *347*, 1260419.

21. Ohtsuki, Y., Fujita, J., Hachisuka, Y., Uomoto, M., Okada, Y., Yoshinouchi, T., Lee, G.H., Furihata, M., and Kohno, N. (2007). Immunohistochemical and immunoelectron microscopic studies of the localization of KL-6 and epithelial membrane antigen (EMA) in presumably normal pulmonary tissue and in interstitial pneumonia. Med. Mol. Morphol. *40*, 198–202.

22. Ishizaka, A., Matsuda, T., Albertine, K.H., Koh, H., Tasaka, S., Hasegawa, N., Kohno, N., Kotani, T., Morisaki, H., Takeda, J., et al. (2004). Elevation of KL-6, a lung epithelial cell marker, in plasma and epithelial lining fluid in acute respiratory distress syndrome. Am. J. Physiol. Lung Cell. Mol. Physiol. *286*, L1088–L1094.

23. Muus, C. (2020). Integrated analyses of single-cell atlases reveal age, gender, and smoking status associations with cell type-specific expression of mediators of SARS-CoV-2 viral entry and highlights inflammatory programs in putative target cells. BioRxiv. https://doi.org/10.1101/2020.04.19.049254.

24. Pamuk, O.N., Can, G., Ayvaz, S., Karaca, T., Pamuk, G.E., Demirtas, S., and Tsokos, G.C. (2015). Spleen tyrosine kinase (Syk) inhibitor fostamatinib limits tissue damage and fibrosis in a bleomycin-induced scleroderma mouse model. Clin. Exp. Rheumatol. *33* (*4, Suppl 91*), S15–S22.

25. McAdoo, S.P., and Tam, F.W. (2011). Fostamatinib Disodium. Drugs Future *36*, 273.

26. Yi, Y.S., Son, Y.J., Ryou, C., Sung, G.H., Kim, J.H., and Cho, J.Y. (2014). Functional roles of Syk in macrophage-mediated inflammatory responses. Mediators Inflamm. *2014*, 270302.

27. Mócsai, A., Ruland, J., and Tybulewicz, V.L. (2010). The SYK tyrosine kinase: a crucial player in diverse biological functions. Nat. Rev. Immunol. *10*, 387–402.

28. Geahlen, R.L. (2014). Getting Syk: spleen tyrosine kinase as a therapeutic target. Trends Pharmacol. Sci. *35*, 414–422.

29. Argade, A., Bhamidipati, S., Li, H., Sylvain, C., Clough, J., Carroll, D., Keim, H., Braselmann, S., Taylor, V., Zhao, H., et al. (2015). Design, synthesis of diaminopyrimidine inhibitors targeting IgE- and IgG-mediated activation of Fc receptor signaling. Bioorg. Med. Chem. Lett. *25*, 2122–2128.

30. Hilgendorf, I., Eisele, S., Remer, I., Schmitz, J., Zeschky, K., Colberg, C., Stachon, P., Wolf, D., Willecke, F., Buchner, M., et al. (2011). The oral spleen tyrosine kinase inhibitor fostamatinib attenuates inflammation and atherogenesis in low-density lipoprotein receptor-deficient mice. Arterioscler. Thromb. Vasc. Biol. *31*, 1991–1999.

31. Newland, A., Lee, E.J., McDonald, V., and Bussel, J.B. (2018). Fostamatinib for persistent/chronic adult immune thrombocytopenia. Immunotherapy *10*, 9–25.

32. Singh, R., Masuda, E.S., and Payan, D.G. (2012). Discovery and development of spleen tyrosine kinase (SYK) inhibitors. J. Med. Chem. *55*, 3614–3643.

33. McAdoo, S.P., Reynolds, J., Bhangal, G., Smith, J., McDaid, J.P., Tanna, A., Jackson, W.D., Masuda, E.S., Cook, H.T., Pusey, C.D., and Tam, F.W. (2014). Spleen tyrosine kinase inhibition attenuates autoantibody production and reverses experimental autoimmune GN. J. Am. Soc. Nephrol. *25*, 2291–2302.

34. Smith, J., McDaid, J.P., Bhangal, G., Chawanasuntorapoj, R., Masuda, E.S., Cook, H.T., Pusey, C.D., and Tam, F.W. (2010). A spleen tyrosine kinase inhibitor reduces the severity of established glomerulonephritis. J. Am. Soc. Nephrol. *21*, 231–236.

35. McAdoo, S.P., Prendecki, M., Tanna, A., Bhatt, T., Bhangal, G., McDaid, J., Masuda, E.S., Cook, H.T., Tam, F.W.K., and Pusey, C.D. (2020). Spleen tyrosine kinase inhibition is an effective treatment for established vasculitis in a pre-clinical model. Kidney Int. *97*, 1196–1207.

36. Kunwar, S., Devkota, A.R., and Ghimire, D.K. (2016). Fostamatinib, an oral spleen tyrosine kinase inhibitor, in the treatment of rheumatoid arthritis: a meta-analysis of randomized controlled trials. Rheumatol. Int. *36*, 1077–1087.

37. Bussel, J., Arnold, D.M., Grossbard, E., Mayer, J., Treliński, J., Homenda, W., Hellmann, A., Windyga, J., Sivcheva, L., Khalafallah, A.A., et al. (2018). Fostamatinib for the treatment of adult persistent and chronic immune thrombocytopenia: results of two phase 3, randomized, placebo-controlled trials. Am. J. Hematol. *93*, 921–930.

38. Weinblatt, M.E., Kavanaugh, A., Genovese, M.C., Musser, T.K., Grossbard, E.B., and Magilavy, D.B. (2010). An oral spleen tyrosine kinase (Syk) inhibitor for rheumatoid arthritis. N. Engl. J. Med. *363*, 1303–1312.

39. Mendes, A.I., Matos, P., Moniz, S., Luz, S., Amaral, M.D., Farinha, C.M., and Jordan, P. (2011). Antagonistic regulation of cystic fibrosis transmembrane conductance regulator cell surface expression by protein kinases WNK4 and spleen tyrosine kinase. Mol. Cell. Biol. *31*, 4076–4086.

40. Na, H.G., Bae, C.H., Choi, Y.S., Song, S.Y., and Kim, Y.D. (2016). Spleen tyrosine kinase induces MUC5AC expression in human airway epithelial cell. Am. J. Rhinol. Allergy *30*, 89–93.

41. Kato, K., Chang, E.H., Chen, Y., Lu, W., Kim, M.M., Niihori, M., Hecker, L., and Kim, K.C. (2020). MUC1 contributes to goblet cell metaplasia and MUC5AC expression in response to cigarette smoke in vivo. Am. J. Physiol. Lung Cell. Mol. Physiol. *319*, L82–L90.

42. Horm, T.M., and Schroeder, J.A. (2013). MUC1 and metastatic cancer: expression, function and therapeutic targeting. Cell Adhes. Migr. *7*, 187–198.

43. Lu, W., Liu, X., Wang, T., Liu, F., Zhu, A., Lin, Y., Luo, J., Ye, F., He, J., Zhao, J., et al. (2020). Elevated MUC1 and MUC5AC mucin protein levels in airway mucus of critical ill COVID-19 patients. J. Med. Virol. https://doi.org/10.1002/jmv.26406.

44. Moore, J.B., and June, C.H. (2020). Cytokine release syndrome in severe COVID-19. Science *368*, 473–474.

45. Zhang, C., Wu, Z., Li, J.W., Zhao, H., and Wang, G.Q. (2020). Cytokine release syndrome in severe COVID-19: interleukin-6 receptor antagonist tocilizumab may be the key to reduce mortality. Int. J. Antimicrob. Agents *55*, 105954.

46. Li, Y.Y., Hsieh, L.L., Tang, R.P., Liao, S.K., and Yeh, K.Y. (2009). Macrophage-derived interleukin-6 up-regulates MUC1, but down-regulates MUC2 expression in the human colon cancer HT-29 cell line. Cell. Immunol. *256*, 19–26.

47. Wilson, J.G. (2020). Cytokine profile in plasma of severe COVID-19 does not differ from ARDS and sepsis. medRxiv. https://doi.org/10.1101/2020.05.15.2010354.

48. d'Alessandro, M., Bergantini, L., Cameli, P., Lanzarone, N., Antonietta Mazzei, M., Alonzi, V., Sestini, P., and Bargagli, E. (2020). Serum KL-6 levels in pulmonary Langerhans' cell histiocytosis. Eur. J. Clin. Invest. *50*, e13242.

49. Braselmann, S., Taylor, V., Zhao, H., Wang, S., Sylvain, C., Baluom, M., Qu, K., Herlaar, E., Lau, A., Young, C., et al. (2006). R406, an orally available spleen tyrosine kinase inhibitor blocks fc receptor signaling and reduces immune complex-mediated inflammation. J. Pharmacol. Exp. Ther. *319*, 998–1008.

50. Hoepel, W., Chen, H.-J., Allahverdiyeva, S., Manz, X., Aman, J., Bonta, P., Brouwer, P., de Taeye, S., Caniels, T., et al.; Amsterdam UMC COVID-19 Biobank (2020). Anti-SARS-CoV-2 IgG from severely ill COVID-19 patients promotes macrophage hyper-inflammatory responses. BioRxiv. https://doi.org/10.1101/2020.07.13.190140.

51. Vogelpoel, L.T., Hansen, I.S., Rispens, T., Muller, F.J., van Capel, T.M., Turina, M.C., Vos, J.B., Baeten, D.L., Kapsenberg, M.L., de Jong, E.C., and den Dunnen, J. (2014). Fc gamma receptor-TLR cross-talk elicits pro-inflammatory cytokine production by human M2 macrophages. Nat. Commun. *5*, 5444.

52. Hoepel, W., Newling, M., Vogelpoel, L.T.C., Sritharan, L., Hansen, I.S., Kapsenberg, M.L., Baeten, D.L.P., Everts, B., and den Dunnen, J. (2019). FcγR-TLR Cross-Talk Enhances TNF Production by Human Monocyte-Derived DCs via IRF5-Dependent Gene Transcription and Glycolytic Reprogramming. Front. Immunol. *10*, 739.

53. Bittker, J.A. (2012). High-Throughput RT-PCR for small-molecule screening assays. Curr. Protoc. Chem. Biol. *4*, 49–63.

54. Pamuk, O.N., Lapchak, P.H., Rani, P., Pine, P., Dalle Lucca, J.J., and Tsokos, G.C. (2010). Spleen tyrosine kinase inhibition prevents tissue damage after ischemia-reperfusion. Am. J. Physiol. Gastrointest. Liver Physiol. *299*, G391–G399.

STAR★METHODS

KEY RESOURCES TABLE

REAGENT or RESOURCE	SOURCE	IDENTIFIER
Antibodies		
Mouse monoclonal anti-MUC1(Clone 214D4)	StemCell Technologies	Cat#: 60137; RRID: AB_118530
Armenian monoclonal hamster anti-MUC1	Abcam	Cat#:ab80952; RRID: AB_1640314
Alexa Fluor 488-conjugated AffiniPure Goat anti-Armenian hamster IgG	Jackson Immunoresearch	Cat# 127-545-099 RRID: AB_2338996
Chemicals, Peptides, and Recombinant Proteins		
Rhodamine Phalloidin	Cytoskeleton	Cat#: PHDR1
SYK inhibitor R788	Rigel Pharmaceuticals	N/A
Caspase 3/7	Thermo Fisher	Cat#: C10423
ROS	Thermo Fisher	Cat#: C10443
DRAQ7	Bio Status	Cat#: DR71000
LOX	sCIVAX	Cat#: LOX-1S
TMRM	Thermo Fisher	Cat#:T668
Critical Commercial Assays		
ABI Cells-to-C_T kit	Thermo Fisher Scientific	Cat#: A35379
CellEvent Caspase 3/7 Green Flow Cytometry Assay Kit	Thermo Fisher	Cat#: C10427
Experimental Models: Cell Lines		
Human: P kidney epithelial cells	[18]	N/A
Experimental Models: Organisms/Strains		
Mouse: C57BL/6J mice	Jackson Laboratories	N/A
Oligonucleotides		
Primer: MUC1 Forward: GGCAGAGAAAGGAAATGGCACATCACT	[18]	N/A
Primer: MUC1 Reverse: CTGCTGCTCCTCACAGTGCTTACAGGT	[18]	N/A
Software and Algorithms		
Harmony High-Content Imaging and Analysis Software	Perkin Elmer	HH17000001
RStudio: Version 1.0.153	RStudio	Rstudio.com
Harmony High-Content Imaging and Analysis Software	Perkin Elmer	HH17000001
GraphPad Prism: Version 7	GraphPad	Graphpad.com
Spotfire Software	Tibco	N/A
Genedata Screener Software	Genedata	Genedata.com
Other		
Opera Phenix High-Content Screening System	Perkin Elmer	HH14000000
Broad Repurposing Library	[17]	N/A

RESOURCE AVAILABILITY

Lead Contact

Further information and requests for resources and reagents should be directed to and will be fulfilled by the Lead Contact, Anna Greka (agreka@bwh.harvard.edu).

Materials Availability
This study did not generate new unique reagents.

Data and Code Availability
This study has not generated new unique data and code.

EXPERIMENTAL MODEL AND SUBJECT DETAILS

Cell Lines
Human P kidney epithelial cells (female) were previously generated from a patient with MUC1 kidney disease.[18] The kidney cell line (P cells) from the patient with ADTKD has one copy of normal MUC1 and one copy of the frameshift mutant (fs). The MUC1-fs lacks normal repeats that might cross react with antibody against the normal anti-VNTR sequence. The cells were maintained at 37°C with 5% CO2 in RenaLife Renal Basal Medium supplemented with RenaLife LifeFactors® (Lifeline Cell Technology), with the exclusion of Gentamycin and Amphotericin B. For all experiments, P cells were maintained below passage 12. The cells were generated with informed consent under WFUHS IRB00014033.

Mice
Adult, 7-week-old male C57BL/6J mice were purchased from Jackson Laboratory (Bar Harbor, ME) and maintained in specific pathogen-free conditions at the Beth Israel Deaconess Medical Center (BIDMC) and allowed to acclimate for 1 week before use in experiments. All mice used in this study were male and 8–12 weeks old. All experimental protocols were performed in accordance with the National Institutes of Health guidelines for the use of experimental animals and were approved by the Institutional Animal Care and Use Committee of BIDMC (Protocol no. 075-2006).

METHOD DETAILS

Broad Repurposing Library
Quality control of The Broad Repurposing Library is performed at the time of plating by LCMS analysis using a Waters Acquity LC System with UV PDA detector and single quad (SQ) mass spectrometer R406 was confirmed present (MS (ESI/SQ) m/z: [M + H]+ Calculated for C22H23FN6O5+H: 471.2; Found: 470.9) in > 97% purity (PDA integration).

Human Protein Atlas
MUC1 immunoperoxidase images were obtained from the Human Protein Atlas with the original source available at the following link: (https://www.proteinatlas.org/ENSG00000185499-MUC1/tissue/lung). mRNA expression data (https://www.proteinatlas.org/ENSG00000185499-MUC1/tissue) were downloaded from the Human Protein Atlas: (http://www.proteinatlas.org/ENSG00000185499.xml).[20] All graphs were visualized using ggplot2.

Fluorescence image acquisition and analysis
All fluorescence imaging performed in this study was done using the Opera Phenix High-Content Screening System (PerkinElmer). For fluorescence imaging of cells (live cell or fixed cell imaging), CellCarrier 384-well Ultra microplates (Perkin Elmer) were used, and a minimum of nine fields was acquired per well using 20x water immersion objectives in a confocal mode.

Image analysis for all imaging experiments was performed using the Harmony software (PerkinElmer). Cell nuclei were first identified using Hoechst staining, and cell number was calculated. Cytoplasmic regions were then detected around each nucleus based on MUC1 channel. The cells from the edge of the field were eliminated from the analysis. For the quantification of MUC1 abundance, the total signal intensity value was calculated in the cell cytoplasm and the average signal per cell was calculated for each well.

For live cell image analysis, caspase 3/7 activation and/or DRAQ7 signal were used to detect cells going through apoptosis and/or cell death, respectively. Single cells were first identified using the digital phase contrast channel and cell number was calculated. Fluorescence intensities were then measured and the threshold for caspase 3/7 and DRAQ7 positive signal was determined. As an output, the number of live (neither caspase3/7 nor DRAQ7 signal detected) cells was calculated in each well at a particular time point.

For the MUC1 membrane prevalence, the images acquired during 10-dose screening were analyzed using the Harmony software STAR morphology feature, which calculates the signal distribution across different cell compartments. The inner side of plasma membrane compartment was analyzed by generating a ''Membrane Profile Image'' (profile 1/5 in Harmony software) (Figure 3B). This function measures the closest distance of a given pixel to a cell border within a width of 4 pixels to preferentially weigh and quantify signal intensity (MUC1) closest to the plasma membrane signal.

For *in vivo* lung imaging, 20x water immersion objective was used, with 5% overlap for entire lung sections. Tissue Image Region for every tissue section was identified based on Gaussian Smoothed filtered global DAPI channel. Every Tissue Image Region was resized to exclude the very peripheral area of the sections. Sliding parabola filtered DAPI channel within the resized tissue area was used to find nuclei; and Phalloidin was used to identify a cytoplasm (see Figure 4B). Mean intensity of MUC1 and Phalloidin was

calculated in each cell, and averaged per cell for the entire tissue sample. The average MUC1 signal was then normalized to Phalloidin signal to take in account variability in slide staining conditions.

High-Content Screening

The automated high-content screening system consisted of robotic arms; plate stackers; a HighRes Pin Tool; Liconic incubators; Biotek plate washers; dedicated Thermo Fisher Combi Multidrop dispensers for each assay reagent; and PerkinElmer High Content Imaging Instrument Opera Phenix, all choreographed by Cellario software. Cell fixation and immunostaining were all performed in a custom-designed light-protected hood (HighRes Biosolutions). Data analysis and representation was performed using Genedata Screener (Genedata AG) and Spotfire (TIBCO).

For the immunofluorescence screen, P cells were seeded 24 h prior to compound treatment at a density of 12,000 cells/well in 384 well CellCarrier Ultra plates (Perkin Elmer), pre-coated with 0.25 mg/mL Synthemax II SC Substrate (Corning). Compounds of the repurposing library set[17] were used at either 5 doses (35, 3.5, 0.35, 0.035 and 0.0035 μM) or 10 doses (16, 5.6, 1.8, 0.6, 0.21, 0.07, 0.02, 0.008, 0.002 and 0.0008 μM) as indicated. The compounds were transferred in replicate from compound source plates to the cell plates using the HighRes Pin Tool. DMSO was used as a negative control and JQ1 (250 nM) (a bromodomain inhibitor) as positive control, based on earlier studies showing potent reduction of total MUC1 mRNA levels (data not shown). After 48 h incubation, cells were fixed 20 min in 4% PFA (Electron Microscopy Sciences) in PBS, washed twice, then permeabilized (10 min) with 0.5% Triton X-100 (Sigma-Aldrich) in PBS and washed once more. Cells were blocked for 10 min at RT with Blocking solution (100mM Tris HCL pH8; 150mM NaCL; 5g/L Blocking Reagent [Roche]), then incubated 90 min at RT with 1:2000, monoclonal mouse anti-MUC1 (214D4) antibody (Millipore) in Roche Blocking solution, followed by four PBS wash cycles. Then the secondary antibody Alexa Fluor® 546 Goat anti-mouse IgG, Thermo Fisher Scientific and Hoechst 33342 stain, Thermo Fisher Scientific, were applied at a 1:1000 dilution in Roche blocking solution and incubated at RT for 45 min, followed by four PBS wash cycles. Plates were then sealed with a Plate Loc plate and stored in a Liconic incubator at 10°C until imaging.

Image acquisition and analysis was as described in the Fluorescence image acquisition and analysis section. Upon image analysis, two parameters were selected, i) total MUC1 cytoplasmic intensity and ii) cell number as was detected by Hoechst 33342 stained nuclei. MUC1 levels in the presence of DMSO or of JQ1 were defined, respectively as 0 and −100% activity. Values for test compounds were normalized accordingly. Cell number was normalized to DMSO control. All compound concentrations showing > −20% reduction in cell number were masked out. Based on ± 3 median absolute deviation value, hit calling criteria for the initial 5 doses screen were chosen as MUC1 reduction > 30% in 2 or more consecutive concentrations for both replicates. For the initial 10 doses screen, dose response curves were generated for each parameter using Genedata Screener (Genedata AG), and positive hits for the profiling screens were selected based on the compound's activity in reducing MUC1 abundance without cell toxicity.

For the RT-PCR-based screen,[53] P cells seeded at 2000 cells/well in 384-well, clear bottom, white wall plates were grown for 24 h, then treated with profiling compounds transferred by pinning to duplicate plates. JQ1 (250 nM) and DMSO were used for controls as above. After 24 h, cells were washed and cDNAs generated using ABI Cells-to-Ct kit (Thermo Fisher Scientific, Waltham, MA). MUC1 and HMBS delta Cp values were determined using a Roche LightCycler 480 Instrument in 5μL reactions using TaqMan probes for MUC1 FAM (4351368 assay ID Hs00159357_m1) and HMBS VIC (4448486- assay ID Hs00609297_m1) (Thermo Fisher Scientific). The fold change effect of the compounds on total MUC1 mRNA was normalized to JQ1 and DMSO controls, as described above.

For the viability profiling screen, P cells were seeded 12 h prior to profiling compound treatment at a density of 12,000 cells/well in 384 well Cell Carrier Ultra plates (Perkin Elmer), pre-coated with 0.25 mg/mL Synthemax II SC Substrate (Corning). After 24 h, CellEvent Caspase-3/7 Green Detection Reagent (Thermo Fisher Scientific) and DRAQ7 (Biostatus) were added at 1:5000 final dilution. Cells were imaged daily during 7 days to monitor viability. Image acquisition was done as described below and viability was assessed as number of live cells at the day 6, when most of DMSO treated wells reached about 95% of confluence.

Administration of SYK inhibitor R788

SYK inhibitor R788 was provided by Rigel Pharmaceuticals (South San Francisco, CA). Mice chow was prepared by Research Diets (New Brunswick, NJ). C57BL/6J mice were fed chow containing 3 g/kg R788 ad libitium for 10 days before experimentation. Control mice were fed normal chow.

Mesenteric Ischemia-Reperfusion (I/R)

All animal procedures were performed in accordance with the guidelines and approval of the Institutional Animal Care and Use Committee (IACUC) of the BIDMC. Mice were randomly assigned to sham or I/R groups and were anesthetized by intraperitoneal injection of 72 mg/kg pentobarbital. Animals were subjected to I/R, as previously described.[54] Mice were anesthetized with 72 mg/kg nembutal (Butler Schein Animal Health) given i.p. Additionally, 36 mg/kg nembuttal was given s.c. during the experiment as needed to maintain anesthesia. All procedures were performed on anesthetized, spontaneously breathing animals with body temperature maintained at 37°C with a controlled heating pad. A midline laparotomy was performed, and the superior mesenteric artery was identified and isolated. Ischemia was induced by application of ~85 g of pressure fir 30 min via a small nontraumatic vascular clamp (Roboz Surgical Instruments, Gaithersburg, MD). After 30 min of ischemia, the clamp was removed, the laparotomy incision was repaired with 4-0 Sofsilk (Covidien, Mansfield, MA), the mice were resuscitated with 1.0 mL of prewarmed sterile PBS s.c., and the intestine was allowed to reperfuse for 180 min. Sham-operated mice were subjected to the same operative procedure as the experimental

group except that clamping of the superior mesenteric artery was not performed. At the conclusion of the reperfusion period, mice were euthanized by carbon dioxide asphyxiation, following the IACUC Guidelines of the BIDMC. Lung removal consisted of intact extraction of the bronchial tree after expansion with tracheal administration of 200–300 of ice-cold 10% phosphate-buffered formalin and fixed overnight in 10% phosphate- buffered formalin at 4°C. Formalin-fixed lung tissues were washed extensively in PBS, processed, and embedded in paraffin for immunohistochemical analysis.

Immunohistochemistry

Immunohistochemical staining was performed on formalin-fixed paraffin sections of lung tissues. The samples were subjected to rehydration and antigen retrieval by overnight immersion in 10mM citric acid buffer (pH 6), for overnight at 60°C. Following antigen retrieval, endogenous peroxidase was blocked with 0.3% H2O2 for 15 min followed by blocking with 2.5% fetal bovine serum (FBS) in PBS for 30 min. Sections were then incubated at 4 C overnight with primary antibodies in 2.5% BSA in PBS ((1:500, monoclonal Armenian hamster anti-MUC1, Abcam; 1:400, Rhodamine Phalloidin, Cytoskeleton Inc). Following washing, the sections were incubated for 1 h at 37°C with secondary antibody diluted in 2.5% BSA in PBS (1:500, Alexa Fluor® 488-conjugated AffiniPure Goat anti-Armenian hamster IgG, Jackson Immunoresearch; 1:500). Slides were washed and mounted in ProLong Gold Antifade Mountant with DAPI (Thermo Fischer Scientific).

QUANTIFICATION AND STATISTICAL ANALYSIS

Statistical analysis was performed and presented using Graphpad Prism version 7.0 software. All data are presented as means ± standard deviation for 'n' experiments unless otherwise specified in the figure legends. The exact value of 'n' for each experiment can be found in the figure legends. Statistical comparisons of two groups for a single variable with normal distributions were analyzed by unpaired t test. Statistical comparisons of two or more groups with one independent variable were analyzed by One-way ANOVA with Tukey post-tests. Statistical comparisons of two or more groups with two independent variables were analyzed by two-way ANOVA with Tukey post-tests. *$p < 0.05$ **$p < 0.01$ ***$p < 0.001$ ****$p < 0.0001$.